Microfluidics of liquid crystals induced by laser radiation

Izabela Śliwa*
Poznan University of Economics and Business, Al. Niepodleglosci 10, 61-875 Poznan, Poland

Pavel V. Maslennikov†
Immanuel Kant Baltic Federal University, Kaliningrad 236040, Str. Universitetskaya 2, Russia

Alex V. Zakharov‡
Saint Petersburg Institute for Machine Sciences, Russian Academy of Sciences, Saint Petersburg 199178, Russia

(Received 26 April 2021; accepted 27 May 2021; published 7 June 2021)

Several scenarios for the formation of hydrodynamic flows in microsized hybrid aligned nematic (HAN) channels, based on the appropriate nonlinear extension of the classical Ericksen-Leslie theory, supplemented by thermomechanical correction of the shear stress and Rayleigh dissipation function, as well as taking into account the entropy balance equation, are analyzed. Detailed numerical simulations were performed to elucidate the role of the heat flux **q** caused by laser radiation focused on the lower boundary of the equally warmed up the HAN channel containing a monolayer of azobenzene with the possibility of a *trans-cis* and *cis-trans* conformational changes in formation of the vortex flow **v**. It is shown that a thermally excited vortex flow is maintained with motion in a positive sense (clockwise) in the vicinity of the orientation defect at the lower boundary of the HAN channel caused by the *trans-cis* and *cis-trans* conformational changes. In the case of the same HAN channel, but without the azobenzene monolayer at the lower boundary, the heat flux **q** can also produce the vortical flow in the vicinity of the laser spot at the lower boundary, directed in a negative sense (counterclockwise). At that, the second vortex is characterized by a much slower speed than the vortical flow in the first case.

DOI: 10.1103/PhysRevE.103.062702

I. INTRODUCTION

The manipulation of molecular liquids or liquid crystals (LCs) in channels ranging in size from tens to hundreds of micrometers has emerged as a separate field called microfluidics [1]. Microfluidics has become a paradigm in various fields from chemical synthesis and biological analysis to optics and information technology and manipulates small (from 10^{-9} to 10^{-18} litres) volumes of fluids. Microfluidics often uses microsized liquid crystal droplets to control the concentration of molecules in biomedical applications [2,3]. Central to the success of microfluidic liquid crystal systems is the development of innovative methods for manipulating liquid crystal systems in microchannels. Pressure gradients [4] and an external electric field [5] for controlling fluid motion are traditionally generated by mechanical, thermomechanical, or electrical drives [6]. On the other hand, the liquid crystals are extremely sensitive to external stimuli and therefore can be used for the construction of stimuli-responsive devices, such as sensors or actuators [6]. They have various advantages in comparison with other types of microsensors and microactuators; simple structure, high shape adaptability, easy downsizing, and low driving voltages. Nematic droplets of the appropriate size, confined in a cylindrical capillary or channel, are microdevices, the orientation of the molecules of which can be manipulated not only by the electric field or pressure, but also by the temperature gradient ∇T. This gradient can be generated, for instance, by a laser beam focused both in the microfluidic volume and at the boundary of the LC channel. One of the principles of liquid crystal pumping is based on the coupling, on the one hand, between the gradient of director field $\nabla \hat{\mathbf{n}}$ and the temperature gradient ∇T, excited, for instance, by a laser beam, focused both at the boundary of the LC channel and inside the LC microvolume, and, on the other hand, between $\nabla \hat{\mathbf{n}}$ and the velocity field **v**, excited in the microfluidic channel by the laser irradiation [7]. In the nematic microfluidic channel, where the director anchoring on the bounding surfaces is the same, i.e., both homogeneously and homeotropically, and when the gradient of the director field $\nabla \hat{\mathbf{n}}$ does not exist, the temperature gradient ∇T generated by the laser beam is not able to excite the hydrodynamic flow **v**, because the driving force is weak enough to set up motion via the Rayleigh-Benard mechanism [7]. The control parameter responsible for the occurrence of motion by the Rayleigh-Benard mechanism is the Rayleigh number $R = \alpha g d^3 \Delta T/(\alpha_4/2\rho)\kappa_\perp$, and the motion occurs at the value $R = R_c \sim 1708$, independent of the fluid under consideration [8]. Here g is the gravitational acceleration, α is the isobaric thermal expansion coefficient, $\alpha_4/2\rho$ corresponds to the kinematic viscosity, and $\kappa_\perp$ is the perpendicular

*izabela.sliwa@ue.poznan.pl
†pashamaslennikov@mail.ru
‡Corresponding author: alexandre.zakharov@yahoo.ca; www.ipme.ru

thermal diffusivity. Whereas the size of the nematic channel is $d \sim 5$–$10\ \mu$m, in this case $R \ll R_c$, and the driving force is weak enough to excite the motion of the LC material via the Rayleigh-Benard mechanism.

Thus, a necessary and sufficient condition for the formation of the hydrodynamic flow $\mathbf{v}$ of LC material in the micro-sized nematic channel is the presence of temperature ∇T and the director field $\nabla \hat{\mathbf{n}}$ gradients, the interaction of which is responsible for the excitation of the flow. The gradient of the director field $\nabla \hat{\mathbf{n}}$ can be set using different anchoring conditions at both boundaries of the LC channel, for instance, homogeneously at one boundary and homeotropically at the opposite boundary, respectively.

We would like to draw attention to another mechanism that allows us to simultaneously form both gradients, the gradient of the director $\nabla \hat{\mathbf{n}}$ and the temperature ∇T fields. This is the photoalignment technique that uses light-induced *trans-cis* and *cis-trans* conformational changes on the surface of azobenzene layers deposited at the boundaries of the micro-sized LC channel [9,10]. It is shown that the charge separation during the conformational changing caused by UV or laser irradiation may lead to the changing of the surface alignment of LC molecules [9], for instance, from homeotropic to planner and vice versa. For example, in the case of an initially homeotropic alignment of the director along the lower boundary of the HAN channel corresponding to the *trans*-conformational state, after laser radiation focused on the lower boundary, a small domain with a planar alignment of the director corresponding to the *cis*-conformational state should appear in the frame of the laser spot. In this case, we are dealing with a sharper reorientation of the director field along the lower boundary of the LC channel, especially near the boundaries of the laser spot, than across the LC channel. At the same time, a local temperature gradient ∇T is formed around the laser spot. Thus, in our case, $\nabla \hat{\mathbf{n}}$ consists of two contributions, the first, weak, due to the reorientation of the director field $\hat{\mathbf{n}}$ across the LC channel, and the second, stronger, due to the sharp reorientation of $\hat{\mathbf{n}}$ in the vicinity of the orientational defect caused by the *trans-cis* conformational transition. Taking into account the fact that the interaction of $\nabla \hat{\mathbf{n}}$ and ∇T leads to the formation of a hydrodynamic flow $\mathbf{v}$, the value of which is proportional to the thermomechanical contribution σ_{zx}^{tm} to the tangential component of the stress tensor σ_{ij} $(i, j = x, z)$ [7,11], it is possible to shed light on the role of the orientational defect caused by the conformational transition and the heat flux $\mathbf{q}$, on the formation of $\mathbf{v}$ in the microsized nematic channel.

The problem of motion of an ultra-small (a few microliters) isotropic and LC drops, under the influence of the temperature gradient, caused by a laser beam, has drawn considerable attention [12–19]. The possibility of using a nearly infrared laser as a microfluidic heat source has been addressed by several groups [13,16]. Laser has the advantages of being fast and easily controlled [20]. Understanding of how the liquid crystal material can be manipulated under the influence of the temperature gradient is also a matter of great fundamental interest, as well as an essential part of knowledge in the field of soft materials science.

We understand that only detailed numerical simulations performed within the framework of the extended Ericksen-Leslie theory [21,22], supplemented by thermomechanical correction of the shear stress tensor and Rayleigh dissipation function, as well as taking into account the entropy balance equation [23], allowed us to recreate the complete picture of the formation of flows in nematic microchannels and capillaries under the effect of the temperature gradient.

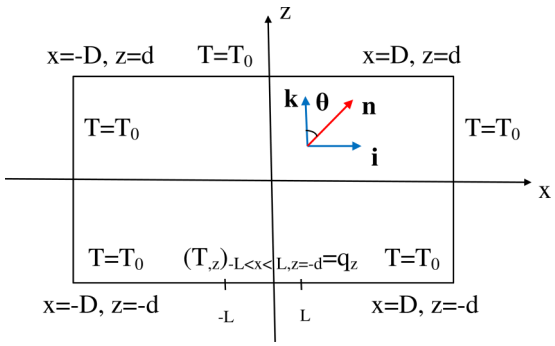

FIG. 1. The coordinate system used for theoretical analysis. The x-axis is taken as being parallel to the director directions on the upper surface, and $\theta(x, z, t)$ is the angle between the director $\hat{\mathbf{n}}$ and the unit vector $\hat{\mathbf{k}}$, respectively. Both the heat flux $\mathbf{q} = q_z\hat{\mathbf{k}}$ and the unit vector $\hat{\mathbf{k}}$ are directed normal to the horizontal boundaries of the LC channel. $2L$ is the size of the laser spot.

The outline of this paper is as follow: the system of hydrodynamic equations describing both the director motion and the fluid flow in the microfluidic HAN channel containing the temperature gradient is given in Sec. II. Numerical results for the number of hydrodynamics regimes, during *trans-cis* and *cis-trans* conformational changes on the bounding surface of the microsized nematic channel and the heat flux across the bounding surfaces of the channel, describing orientational relaxation of the director, velocity, and temperature are given in Sec. III. Conclusions are summarized in Sec. IV.

II. FORMULATION OF THE BALANCE EQUATIONS

To elucidate the role of the heat flux $\mathbf{q} = q_z\hat{\mathbf{k}}$ caused by laser radiation focused on the lower boundary of a uniformly heated microsized nematic channel containing a monolayer of azobenzene with the possibility of *trans-cis* and *cis-trans* conformational changes in exciting of the hydrodynamic flow $\mathbf{v} = u\hat{\mathbf{i}} + w\hat{\mathbf{k}}$, it is necessary to investigate the growth of the director $\hat{\mathbf{n}}$ and the temperature T gradients in the vicinity of the laser spot. With this in mind, we consider a two-dimensional nematic channel consisting of asymmetric polar molecules, such as cyanobiphenyls, with a density of ρ and bounded by two horizontal and two lateral surfaces at mutual distances of $2d$ and $2D$ $(D \gg d)$, respectively, on a scale of the order of micrometers. The coordinate system defined by our task assumes that the director $\hat{\mathbf{n}} = (n_x, 0, n_z) = \sin\theta\hat{\mathbf{i}} + \cos\theta\hat{\mathbf{k}}$ is in the XZ plane (see Fig. 1), where $\hat{\mathbf{i}}$ is the unit vector directed parallel to the horizontal restricted surfaces, which coincides with the planar director orientation on the upper boundary $(\hat{\mathbf{i}} \parallel \hat{\mathbf{n}}_{z=d})$, whereas the unit vector $\hat{\mathbf{k}}$ is directed parallel to the lateral restricted surfaces, which coincides with the planar director orientation on these surfaces $(\hat{\mathbf{k}} \parallel \hat{\mathbf{n}}_{x=\pm d})$, $\theta \equiv \theta(x, z, t)$ denotes the polar angle, i.e., the angle between the direction of the director $\hat{\mathbf{n}}$ and the unit vector $\hat{\mathbf{k}}$, and $\hat{\mathbf{j}} = \hat{\mathbf{k}} \times \hat{\mathbf{i}}$.

Moreover, we will work with the dimensionless space variables $\bar{x} = \frac{x}{d}$ and $\bar{z} = \frac{z}{d}$, and in the following equations the overbars will be eliminated, and the ratio of the channel length to its width D/d will be chosen being equal to 10.

In our 2D hybrid aligned nematic (HAN) channel with the planar orientation on the upper and lateral surfaces and the homeotropic orientation on the lower boundary containing the monolayer of azobenzene in the *trans* conformational state before it is exposed to focused laser radiation, the boundary conditions for the director field $\hat{\mathbf{n}}$ can be written in the form

$$(n_x)_{x=\pm 10,-1\leqslant z\leqslant 1} = 0, \quad (n_x)_{-10<x<10,z=1} = 1, \quad (n_x)_{-10<x<10,z=-1} = 0. \tag{1}$$

In order to clarify the role of *trans-cis* conformational transition in formation of the hydrodynamic flow in the microsized HAN channel, we consider the orientational defect on the lower boundary containing the monolayer of azobenzene. In this case, the lower boundary is heated by the laser beam focused on the lower surface at the point $z = -1$, $x = x_0$, and the heat flux $\mathbf{q} = q_z\hat{\mathbf{k}}$ to the HAN channel can be written as

$$q_z = \mathcal{Q}_z \exp\left(-\frac{2(x-x_0)^2}{\Delta^2}\right)\mathcal{H}[t_{\text{in}} - t], \tag{2}$$

where $\mathcal{Q}_z$ is the dimensionless heat flux coefficient, $\mathcal{H}[t_{\text{in}} - t]$ is the Heaviside step function, t_{in} is the duration of the energy injection into the LC sample, and $\Delta = 2L$ is the Gaussian spot size (see Fig. 1), respectively. The azobenzene monolayer deposited on the nematic boundary, which in the initial state exhibits the *trans* conformation, with the transmittance of a He-Ne laser beam, undergoes the *trans-cis* isomerization [9]. By putting, for instance, the 6Az10PVA monolayer in contact with the polar LC phase, such as 4-*n*-pentyl-4′-cyanobiphenyl (5CB), one can expect the change, during the laser beam transmittance, of the surface alignment of the 5CB molecules from homeotropic to planar. Such an orientational transition, in turn, can be induced by changing of the surface charge density caused by the charge separation, taking place during the conformational change on the surface azobenzene monolayer. With this in mind, we consider the orientational defect on the lower bounding surface, which is characterized by continuous change of the director's orientation along the length of the lower boundary, from homeotropic to planar, and again to homeotropic orientation. So the microsized HAN channel contains an additional gradient of $\nabla\hat{\mathbf{n}}$ on the lower boundary:

$$(n_x)_{x=\pm 10,-1\leqslant z\leqslant 1} = 0, (n_x)_{-10<x<10,z=1} = 1, \quad (n_x)_{-10<x<-l,z=-1} = (n_x)_{l<x<10,z=-1} = 0, \quad (n_x)_{-l<x<l,z=-1} = \sin\mathcal{A}, \tag{3}$$

where $\mathcal{A} = \tan^{-1}(\frac{l^2-x^2}{4x^4})$, $l = \frac{L}{D}$ is the dimensionless size of the laser spot, and $2L$ is the length of the orientational defect on the lower boundary with the director's orientation changing continuously from the homeotropic to planar, and again to homeotropic orientation, whereas on the rest length of that surface there is the homeotropic director's orientation ($\hat{\mathbf{k}} \parallel \hat{\mathbf{n}}_{z=-1}$). It should be noticed that the length $2L$ of the orientational defect is equal to the Gaussian spot size Δ.

In order to be able to observe the formation of the hydrodynamic flow $\mathbf{v}$ in the HAN channel under the effect of the heat flux $\mathbf{q}$ when heating occurs for some time t_{in}, let us consider a set of the balance equations: first, the torque balance equation [7,15,18]

$$\left[\frac{\delta\mathcal{W}_F}{\delta\hat{\mathbf{n}}} + \frac{\delta\mathcal{R}^{\text{vis}}}{\delta\hat{\mathbf{n}}_{,t}} + \frac{\delta\mathcal{R}^{tm}}{\delta\hat{\mathbf{n}}_{,t}}\right] \times \hat{\mathbf{n}} = 0, \tag{4}$$

second, the linear momentum balance equation [15,18]

$$\rho\frac{d\mathbf{v}}{dt} = \nabla\cdot\sigma, \tag{5}$$

and, third, the entropy balance equation [15,18]

$$\rho_m C_P\frac{dT}{dt} = -\nabla\cdot\mathbf{q}, \tag{6}$$

respectively. Here $\mathcal{W}_F = \frac{1}{2}[K_1(\nabla\cdot\hat{\mathbf{n}})^2 + K_3(\hat{\mathbf{n}}\times\nabla\times\hat{\mathbf{n}})^2]$ is the elastic energy density, K_1 and K_3 are the splay and bend elastic constants of the nematic phase, $\sigma = \sigma^{el} + \sigma^{\text{vis}} + \sigma^{tm} - P\mathcal{I}$ is the full stress tensor (ST), and $\sigma^{el} = -\frac{\partial\mathcal{W}_F}{\partial\nabla\hat{\mathbf{n}}}\cdot(\nabla\hat{\mathbf{n}})^T$, $\sigma^{\text{vis}} = \frac{\delta\mathcal{R}^{\text{vis}}}{\delta\nabla\mathbf{v}}$, and $\sigma^{tm} = \frac{\delta\mathcal{R}^{tm}}{\delta\nabla\mathbf{v}}$ are the ST components corresponding to the elastic, viscous, and thermomechanical forces, respectively, whereas P is the dimensional hydrostatic pressure in the HAN system and $\mathcal{I}$ is the unit tensor. In turn, $\mathbf{q} = -T\frac{\delta\mathcal{R}}{\delta\nabla T}$ is the heat flux in the nematic phase, C_P is the heat capacity of the LC system, and ρ_m is the mass density of the nematic system.

In this case the dimensionless analog of the torque balance equation can be written in the form [7,15,18]

$$\begin{aligned} n_z n_{x,\tau} - n_x n_{z,\tau} = {} & n_z\mathcal{A}_{0,x} - n_x\mathcal{A}_{0,z} + K(n_z h_{,z} + n_x h_{,x}) \\ & - \tfrac{1}{2}\Delta\psi + 2\gamma\psi_{,xz}n_x n_z \\ & + \gamma(\psi_{,zz} - \psi_{,xx})\left(n_x^2 - n_z^2\right) \\ & + \psi_{,z}\mathcal{N}_x + \psi_{,x}\mathcal{N}_z + \delta_1(\chi_{,x}\mathcal{L}_x + \chi_{,z}\mathcal{L}_z), \end{aligned} \tag{7}$$

where $\tau = (K_1/\gamma_1 d^2)t$ is the dimensionless time, $K = K_3/K_1$, $\gamma = \gamma_2/\gamma_1$, γ_1 and γ_2 are the rotational viscosity coefficients, $\mathcal{A}_0 = n_{x,x} + n_{z,z}$, $\bar{z} = \frac{z}{d}$ is the dimensionless distance away from the center of the HAN channel, $\bar{x} = \frac{x}{L}$ is the dimensionless space variable corresponding to the x-axis, $\bar{\psi} = \frac{\gamma_1 d}{K_1}\psi$ is the scaled analog of the stream function ψ for the velocity field $\mathbf{v} = u\hat{\mathbf{i}} + w\hat{\mathbf{k}} = -\nabla\times\hat{\mathbf{j}}\psi$ (see Ref. [15]), $n_{z,\tau} = \frac{\partial n_z}{\partial\tau}$, $\mathcal{N}_x = n_x n_{z,x} - n_z n_{x,x}$, $\mathcal{N}_z = n_z n_{x,z} - n_x n_{z,z}$, $\mathcal{L}_x = n_x n_{z,x} - \frac{3}{2}n_z n_{x,x} + \frac{1}{2}n_x n_{x,z}$, and $\mathcal{L}_z = -n_z n_{x,z} + \frac{3}{2}n_x n_{z,z} + \frac{1}{2}n_z n_{z,x}$. Here $\delta_1 = \frac{T_{NI}}{K_1}\xi$ is the parameter of the nematic system, and $\xi = 10^{-12}$ J/mK is the thermomechanical constant [7,11].

The dimensionless linear balance equation for the velocity field $\mathbf{v} = u\hat{\mathbf{i}} + w\hat{\mathbf{k}} = -\nabla\times\hat{\mathbf{j}}\psi$ takes the form [15,18]

$$\begin{aligned} \delta_2\psi_{,xz\tau} = {} & a_1\psi_{,zzzz} + a_2\psi_{,xzzz} + a_3\psi_{,xxzz} \\ & + a_4\psi_{,xxxz} + a_5\psi_{,xxxx} + a_6\psi_{,zzz} \\ & + a_7\psi_{,xzz} + a_8\psi_{,xxz} + a_9\psi_{,xxx} + a_{10}\psi_{,zz} \\ & + a_{11}\psi_{,xz} + a_{12}\psi_{,xx} + \mathcal{F}, \end{aligned} \tag{8}$$

whereas the dimensionless entropy balance can be written as [15,18]

$$\begin{aligned}\delta_3\chi_{,\tau} = &\left[\chi_{,x}\left(\lambda n_x^2 + n_z^2\right) + (\lambda-1)n_x n_z \chi_{,z}\right]_{,x} \\ &+ \left[\chi_{,z}\left(\lambda n_z^2 + n_x^2\right) + (\lambda-1)n_x n_z \chi_{,x}\right]_{,z} \\ &- \delta_3(\psi_{,z}\chi_{,x} - \psi_{,x}\chi_{,z}). \end{aligned} \tag{9}$$

Here $\lambda = \lambda_\parallel/\lambda_\perp$ is the dimensionless parameter, and $\lambda_\perp$ and $\lambda_\parallel$ are the heat conductivity coefficients perpendicular and parallel to the director, respectively. It should be noted that the function $\mathcal{F} = (\sigma_{xx}^{el} + \sigma_{xx}^{tm} - \sigma_{zz}^{el} - \sigma_{zz}^{tm})_{,xz} + (\sigma_{zx}^{el} + \sigma_{zx}^{tm})_{,zz} - (\sigma_{xz}^{el} + \sigma_{xz}^{tm})_{,xx}$, the coefficients $a_i (i = 1, \ldots, 12)$, and the functions σ_{ij}^{tm} $(i, j = x, z)$ and σ_{ij}^{el} $(i, j = x, z)$ are given in Ref. [18], whereas $\sigma_{ij} = \sigma_{ij}^{el} + \sigma_{ij}^{\rm vis} + \sigma_{ij}^{tm} - \mathcal{P}\delta_{ij}$ $(i, j = x, z)$ is the stress tensor (ST) of the nematic system, $\mathcal{P} = \frac{d^2}{K_1}P$ is the dimensionless hydrostatic pressure in the HAN channel, and σ_{ij}^{el}, $\sigma_{ij}^{\rm vis}$, and σ_{ij}^{tm} are the dimensionless ST components corresponding to the elastic, viscous, and thermomechanical forces, respectively. The set of the rest parameters of the nematic system, corresponding to the case of 4-cyano-4′-pentylbiphenyl (5CB), are $\delta_2 = \frac{\rho K_1}{\gamma_1^2}$ and $\delta_3 = \frac{\rho C_p K_1}{\gamma_1 \lambda_\perp}$.

The dimensionless balance Eqs. (7)–(9) can be derived from the dimensionless balance of elastic $\mathbf{T}_{el} = \frac{\delta \mathcal{W}_F}{\delta \hat{\mathbf{n}}} \times \hat{\mathbf{n}}$, viscous $\mathbf{T}_{\rm vis} = \frac{\delta \mathcal{R}^{\rm vis}}{\delta \hat{\mathbf{n}}_{,\tau}} \times \hat{\mathbf{n}}$, and thermomechanical $\mathbf{T}_{tm} = \frac{\delta \mathcal{R}^{tm}}{\delta \hat{\mathbf{n}}_{,\tau}} \times \hat{\mathbf{n}}$ torques [7,15,24], where $\mathcal{W}_F = \frac{1}{2}[(\nabla\cdot\hat{\mathbf{n}})^2 + K(\hat{\mathbf{n}}\times\nabla\times\hat{\mathbf{n}})^2]$ is the dimensionless elastic energy density and $\hat{\mathbf{n}}_{,\tau} \equiv \frac{d\hat{\mathbf{n}}}{d\tau}$ is the material derivative of $\hat{\mathbf{n}}$, whereas $2\gamma_1\mathcal{R}^{\rm vis} = \alpha_1(\hat{\mathbf{n}}\cdot\mathbf{B}_{\rm s}\cdot\hat{\mathbf{n}})^2 + \gamma_1(\hat{\mathbf{n}}_{,\tau} - \mathbf{B}_{\rm a}\cdot\hat{\mathbf{n}})^2 + 2\gamma_2(\hat{\mathbf{n}}_{,\tau} - \mathbf{B}_{\rm a}\cdot\hat{\mathbf{n}})\cdot[\mathbf{B}_{\rm s}\cdot\hat{\mathbf{n}} - (\hat{\mathbf{n}}\cdot\mathbf{B}_{\rm s}\cdot\hat{\mathbf{n}})\hat{\mathbf{n}}] + \alpha_4\mathbf{B}_{\rm s} : \mathbf{B}_{\rm s} + (\alpha_5+\alpha_6)(\hat{\mathbf{n}}\cdot\mathbf{B}_{\rm s}\cdot\mathbf{B}_{\rm s}\cdot\hat{\mathbf{n}})^2$ is the viscous, and $\delta_1\mathcal{R}^{tm} = (\hat{\mathbf{n}}\cdot\nabla\chi)\mathbf{B}_{\rm s} : \mathbf{A} + \nabla\chi\cdot\mathbf{B}_{\rm s}\cdot\mathbf{A}\cdot\hat{\mathbf{n}} + (\hat{\mathbf{n}}\cdot\nabla\chi)[\hat{\mathbf{n}}_{,\tau} - \mathbf{B}_{\rm a}\cdot\hat{\mathbf{n}} - 3\mathbf{B}_{\rm s}\cdot\hat{\mathbf{n}} + 3(\hat{\mathbf{n}}\cdot\mathbf{B}_{\rm s}\cdot\hat{\mathbf{n}})\hat{\mathbf{n}}]\cdot\mathbf{A}\cdot\hat{\mathbf{n}} + \hat{\mathbf{n}}(\nabla\mathbf{v})^T\cdot\mathbf{A}\cdot\nabla\chi + \frac{1}{2}(\hat{\mathbf{n}}\cdot\mathbf{B}_{\rm s}\cdot\hat{\mathbf{n}})\nabla\chi\cdot\mathbf{A}\cdot\hat{\mathbf{n}} + \hat{\mathbf{n}}_{,\tau}\cdot\mathbf{A}\cdot\nabla\chi + \frac{1}{2}\mathcal{A}_0\nabla\chi\cdot\nabla\mathbf{v}\cdot\hat{\mathbf{n}} + (\hat{\mathbf{n}}\cdot\nabla\chi)\mathcal{A}_0(\hat{\mathbf{n}}\cdot\mathbf{B}_{\rm s}\cdot\hat{\mathbf{n}}) + \frac{1}{2}\mathcal{A}_0\hat{\mathbf{n}}_{,\tau}\cdot\nabla\chi$ is the thermomechanical contribution to the full dimensionless Rayleigh dissipation function [7,15,18]. Here $\mathbf{B}_{\rm s} = \frac{1}{2}[\nabla\mathbf{v} + (\nabla\mathbf{v})^T]$ and $\mathbf{B}_{\rm a} = \frac{1}{2}[\nabla\mathbf{v} - (\nabla\mathbf{v})^T]$ are the symmetric and asymmetric contributions, respectively, to the rate of strain tensor, $\mathbf{A} = \frac{1}{2}[\nabla\hat{\mathbf{n}} + (\nabla\hat{\mathbf{n}})^T]$, $\mathcal{A}_0 = \nabla\cdot\hat{\mathbf{n}}$ is the scalar invariant of the tensor $\mathbf{A}$, $(\nabla\hat{\mathbf{n}})^T$ is the transposition of $\nabla\hat{\mathbf{n}}$, $\chi \equiv \chi(x,z,\tau) = T(x,z,\tau)/T_{NI}$ is the dimensionless temperature, T_{NI} is the nematic-isotropic transition temperature, and α_i $(i = 1$–$6)$ are the Leslie viscosity coefficients. We use here the invariant, multiple dot convention: $\mathbf{ab} = a_i b_j$, $\mathbf{a}\cdot\mathbf{b} = a_i b_i$, $\mathbf{A}\cdot\mathbf{B} = A_{ik}B_{kj}$, and $\mathbf{A} : \mathbf{B} = A_{ik}B_{ki}$, where repeated Cartesian indices are summed.

We consider the HAN channel with the heat flux $\mathbf{q} = q_z\hat{\mathbf{k}}$ across the lower boundary caused by the laser beam. In dimensionless form, it is written as

$$[\chi_{,z}(x,z,\tau)]_{-l<x<l,z=-1} = \mathcal{Q}_z, \tag{10}$$

whereas on the rest boundaries the temperature is kept constant:

$$\begin{aligned}\chi_{-10<x<-l,z=-1} &= \chi_{l<x<10,z=-1} = \chi_{x=\pm10,-1<z<1} \\ &= \chi_{-10<x<10,z=1} = \chi_0. \end{aligned} \tag{11}$$

Here $\chi_{,\alpha} = \frac{\partial\chi}{\partial\alpha}$ $(\alpha = x, z)$, and $\chi_0 = T_0/T_{NI}$ is the dimensionless temperature outside the laser spot. Physically, this means that in the HAN channel the temperature gradient $\nabla\chi$ may be built up by the laser radiation focused on the lower boundary.

Taking into account that the width of the nematic channel $d \sim 1$–$5\ \mu$m, one can assume that the mass density $\rho_m =$ const across the HAN channel, and one deals with an incompressible fluid. In turn, the incompressibility condition $\nabla\cdot\mathbf{v} = 0$ assumes that

$$u_{,x} + w_{,z} = 0, \tag{12}$$

where $u \equiv v_x(x,z,\tau) = \psi_{,z}$ and $w \equiv v_z(x,z,\tau) = -\psi_{,x}$ are the components of the vector $\mathbf{v} = u\hat{\mathbf{i}} + w\hat{\mathbf{k}}$, and $u_{,\alpha} = \frac{\partial u}{\partial\alpha}$ $(\alpha = x, z)$.

Now the evolution of the director in the HAN channel confined between two horizontal and two vertical solid surfaces, under the influence of viscous, elastic, and thermomechanical forces and taking into account the flow, can be obtained by solving the system of the nonlinear partial differential Eqs. (7), (8), and (10) with the appropriate dimensionless boundary conditions for the director $\hat{\mathbf{n}}$ or the polar angle θ [see Eqs. (1) and (3)], velocity field $\mathbf{v} = u\hat{\mathbf{i}} + w\hat{\mathbf{k}} = -\nabla\times\hat{\mathbf{j}}\psi$:

$$\begin{aligned} u_{-10<x<10,z=-1} &= (\psi_{,z})_{-10<x<10,z=-1} = u_{x=-10,-1\leqslant z<1} \\ &= (\psi_{,z})_{x=-10,-1\leqslant z<1} = 0, \\ u_{x=10,-1\leqslant z<1} &= (\psi_{,z})_{-10\leqslant x\leqslant 10,z=1} = u_{-10\leqslant x\leqslant 10,z=1} \\ &= (\psi_{,z})_{-10\leqslant x\leqslant 10,z=1} = 0, \\ w_{-10<x<10,z=-1} &= (\psi_{,x})_{-10<x<10,z=-1} = w_{x=-10,-1\leqslant z<1} \\ &= (\psi_{,x})_{x=-10,-1\leqslant z<1} = 0, \\ w_{x=10,-1\leqslant z<1} &= (\psi_{,x})_{x=10,-1\leqslant z<1} = w_{-10\leqslant x\leqslant 10,z=1} \\ &= (\psi_{,x})_{-10\leqslant x\leqslant 10,z=1} = 0, \end{aligned} \tag{13}$$

temperature field $\chi(x,z,\tau)$ [see Eqs. (10) and (11)], and the initial condition taken in the form

$$\hat{\mathbf{n}}(x,z,\tau=0) = \hat{\mathbf{n}}_{el}^{in}(x,z). \tag{14}$$

For the case of 4-cyano-4′-pentylbiphenyl (5CB), at temperature corresponding to nematic phase, the first three parameters $\delta_1 = \frac{T_{NI}}{K_1}\xi$, $\delta_2 = \frac{\rho_m K_1}{\gamma_1^2}$, and $\delta_3 = \frac{\rho_m C_p K_1}{\gamma_1\lambda_\perp}$, which are involved in Eqs. (7)–(9), have the following values: $\delta_1 \sim 30.7$, $\delta_2 \sim 2.0\times10^{-6}$, and $\delta_3 \sim 6.0\times10^{-4}$.

For calculations, the value of the density ρ was chosen to be equal to 10^3 kg/m^3, whereas both the Frank elastic coefficient K_1 and the RVC γ_1 were chosen as $\sim$10 pN [24] and $\sim$0.071 Pa s [25], respectively. The value of the heat conductivity coefficient $\lambda_\perp$ is equal to $\sim$0.24 W/m K [26], whereas the measured value of the specific heat C_p is equal to $\sim10^3$ J/kg K [27].

Using the fact that $\delta_2 \ll 1$, Eq. (8) can be considerably simplified and takes the form [15,18]

$$\begin{aligned} &a_1\psi_{,zzzz} + a_2\psi_{,xzzz} + a_3\psi_{,xxzz} + a_4\psi_{,xxxz} \\ &\quad + a_5\psi_{,xxxx} + a_6\psi_{,zzz} \\ &\quad + a_7\psi_{,xzz} + a_8\psi_{,xxz} + a_9\psi_{,xxx} + a_{10}\psi_{,zz} \\ &\quad + a_{11}\psi_{,xz} + a_{12}\psi_{,zz} + \mathcal{F} = 0, \end{aligned} \tag{15}$$

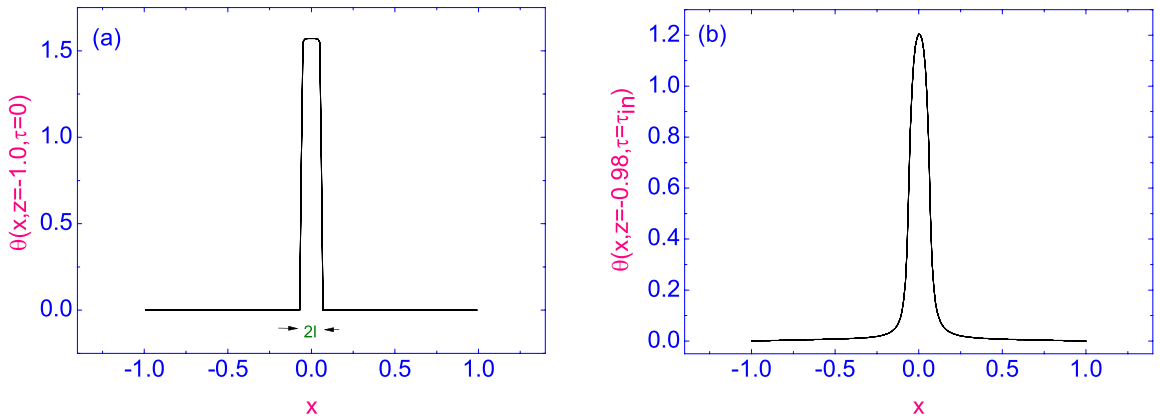

FIG. 2. (a) The initial distribution of the polar angle $\theta(-1.0 \leqslant x \leqslant 1.0, z = -1.0, \tau = 0)$ in the vicinity of the laser spot ($\Delta = 2l = 0.1$). (b) The stationary distribution of the polar angle $\theta(-1.0 \leqslant x \leqslant 1.0, z = -0.98, \tau = \tau_{\text{in}})$ (in rad) along the width ($-1.0 \leqslant x \leqslant 1.0$) of the HAN channel in the vicinity of the lower ($z = -0.98$) boundary.

where a_i ($i = 1, \ldots, 12$) and $\mathcal{F}$ are functions which have been defined in Refs. [15,18].

III. NUMERICAL RESULTS FOR TWO CASES OF THE DIRECTOR ANCHORING IN HAN CHANNEL

First, we will focus on the problem of how the simultaneous increase in the gradients of the director $\hat{\mathbf{n}}$ and temperature χ fields caused by laser radiation affects the nature of the evolution of the director $\hat{\mathbf{n}}(x, z, \tau)$ [or the polar angle $\theta(x, z, \tau)$] to its stationary distribution $\hat{\mathbf{n}}_{st}(x, z) = \hat{\mathbf{n}}(x, z, \tau = \tau_{\text{in}})$ in the vicinity of the orientational defect.

A. Case A

In this case $\nabla\hat{\mathbf{n}}$ consists of two contributions, the first, weak, due to the reorientation of the director field $\hat{\mathbf{n}}$ across the LC channel, and the second, stronger, due to the sharp reorientation of $\hat{\mathbf{n}}$ in the vicinity of the orientational defect, caused by the *trans-cis* conformational transition. Taking into account the fact that the interaction of $\nabla\hat{\mathbf{n}}$ and $\nabla\chi$ leads to the formation of a hydrodynamic flow $\mathbf{v}$, the value of which is proportional to the thermomechanical contribution σ_{zx}^{tm} to the tangential component of the stress tensor, it is possible to shed light on the role of the orientational defect caused by the conformational transition and the heat flux $\mathbf{q}$, on the formation of $\mathbf{v}$ in the microsized nematic channel.

It can be obtained by solving the system of the nonlinear partial differential Eqs. (7), (15), and (9), together with the boundary conditions (3), (10), (11), (13), and (14) (hereafter referred to as case A), by means of the sweep method [28]. Notice that the initial distribution of the angle $\theta_{el}^{in}(x, z)$ has been obtained from Eq. (7) by means of the relaxation method [29], with $u_{,x} = u_{,z} = w_{,x} = w_{,z} = \chi_{,x} = \chi_{,z} = 0$, and with the boundary conditions in the form of Eqs. (3), (10), and (11), whereas the initial condition for the polar angle $\theta_{el}(x, z, \tau = 0)$ is chosen in the form

$$\theta_{el}(x, z, \tau = 0) = \begin{cases} 0, & \text{at } -10 \leqslant x < -l,\ l < x \leqslant 10, \text{ and } -1 \leqslant z \leqslant 1, \\ \frac{\pi}{2}, & \text{at } -l \leqslant x \leqslant l \text{ and } -1.0 \leqslant z \leqslant 1.0. \end{cases}$$

In the calculations, the relaxation criterion $\epsilon = |(\theta_{(m+1)}(x, z, \tau) - \theta_{(m)}(x, z, \tau))/\theta_{(m)}(x, z, \tau)|$ was chosen to be equal to 10^{-4}, and the numerical procedure was then carried out until a prescribed accuracy was achieved. Here m is the iteration number and τ_R is the relaxation time of the system.

It should be clarified once again that the initial condition for the polar angle $\theta_{el}(x, z, \tau = 0)$ was chosen to calculate the initial distribution of the director $\hat{\mathbf{n}}(x, z, \tau = 0) = \hat{\mathbf{n}}_{el}^{in}(x, z)$ field only under the action of elastic forces.

Plots of the polar angle $\theta(x, z, \tau = \tau_{\text{in}})$ both along the width ($-1.0 \leqslant x \leqslant 1.0, z = -0.98$) and across ($x = 0.0$, $-1.0 \leqslant z \leqslant 1.0$) the HAN channel, when the heating occurs during some time $\tau_5 = \tau_{\text{in}}$, are shown in Figs. 2(a) and 2(b) and Figs. 3(a) and 3(b), respectively. According to our calculations, the highest value of $|\nabla\theta(x, z)|$ is reached in the vicinity of the lower ($-l + \delta < x < l - \delta, z = -1.0$) boundary. Here $l = \pm 0.05$ are the right and left ends of the orientational defect on the lower boundary, where the homeotropic director's orientation transits to the homogeneous, and $\delta \ll l$ is a small number.

It should be noted that in case A, the values of the dimensionless heat flux coefficient $\mathcal{Q}_z d/T_{NI}\lambda_\perp$ and the dimensionless injection time $\tau_{\text{in}} = \frac{K_1}{\gamma_1 d^2} t_{\text{in}}$ are 0.18 ($\sim 1.5\times 10^{-3}$ mW/μm^2) and 10^{-4} (~ 0.18 ms), respectively.

Now we would like to draw attention to a mechanism that allows us to simultaneously set up the temperature gradient $\nabla\chi$ and complicate the gradient of the director $\nabla\hat{\mathbf{n}}$, composed of the existing contribution, due to the hybrid alignment of nematic phase and an additional contribution, due to the variation of the director field $\hat{\mathbf{n}}$ along the local domain containing the orientational defect. This is the photoalignment

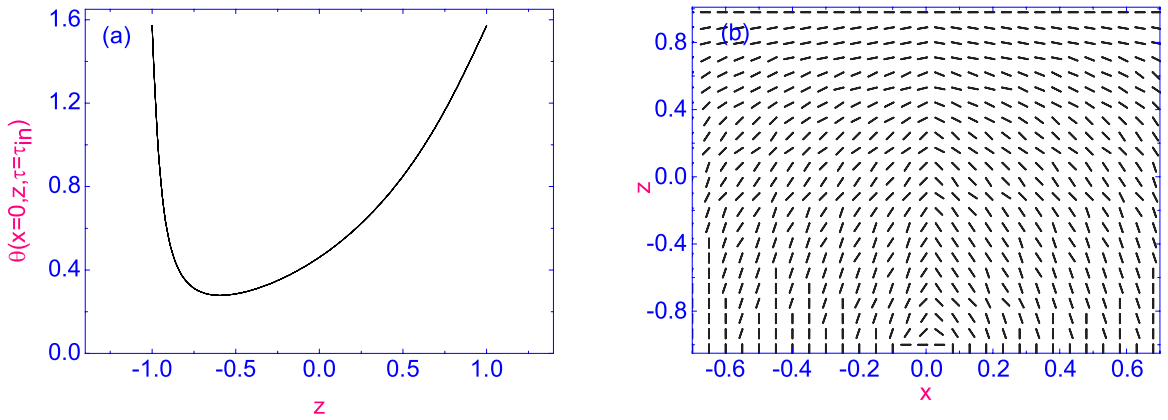

FIG. 3. (a) The stationary distribution of the polar angle $\theta(x = 0, -1.0 \leqslant z \leqslant 1.0, \tau = \tau_{\rm in})$ (in rad) across the middle part ($x = 0$) of the HAN channel. (b) Fragment of the stationary distribution of the director field $\hat{\mathbf{n}}_{st}(x, z) = \hat{\mathbf{n}}(x, z, \tau = \tau_{\rm in})$ in the vicinity of the laser spot. The Gaussian spot size $\Delta = 2l = 0.1$ and $\tau_{\rm in} = 10^{-4}$.

mechanism that uses light-induced *trans-cis* and *cis-trans* conformational changes on the surface of azobenzene layers deposited at the boundaries of the microsized LC channel [9,10]. It is shown that the charge separation during the conformational changing caused by laser irradiation may lead to the change of the surface alignment of 5CB molecules, from homeotropic to plannar and vice versa [9]. In our case there is the initially homeotropic alignment of the director along the lower boundary of the HAN channel corresponding to the *trans*-conformational state. After laser radiation focused on the lower boundary, a small domain with a planar alignment of the director corresponding to the *cis*-conformational state should appear in the frame of the laser spot. In this case, there is a sharper reorientation of the director field along the lower boundary of the HAN channel, especially near the boundaries of the laser spot, than across the HAN channel [see Figs. 2(a) and 2(b) and Figs. 3(a) and 3(b), respectively]. At the same time, the local temperature gradient $\nabla\chi$ is set up around the laser spot [see Figs. 4(a) and 4(b), respectively]. Thus, in our case, $\nabla\hat{\mathbf{n}}$ consists of two contributions, the first, weak, due to the reorientation of the director field $\hat{\mathbf{n}}$ across the HAN channel, and the second, stronger, due to the sharp reorientation of $\hat{\mathbf{n}}$ in the vicinity of the orientational defect caused by the *trans-cis* and *cis-trans* conformational transition. Taking into account the fact that the interaction of $\nabla\hat{\mathbf{n}}$ and $\nabla\chi$ leads to the formation of a hydrodynamic flow $\mathbf{v}$, the value of which is proportional to the thermomechanical contribution σ_{zx}^{tm} to the tangential component of the stress tensor, it is possible to shed light on the role of the orientational defect caused by the conformational transition and the heat flux $\mathbf{q}$, on the formation of $\mathbf{v}$ in the microsized HAN channel.

The relaxation of both the vertical $w(x, z, \tau)$ and the horizontal $u(x, z, \tau)$ components of the velocity $\mathbf{v} = u(x, z, \tau)\hat{\mathbf{i}} + w(x, z, \tau)\hat{\mathbf{k}}$ to their stationary distributions $w(x, z, \tau = \tau_{\rm in})$ and $u(x, z, \tau = \tau_{\rm in})$, respectively, are shown in Figs. 5(a) and 5(b). According to our calculations the highest value of $\mathbf{v}$ is reached in the vicinity of the hotter lower ($z = -0.98$) boundary, at both the left and right-hand sides of the orientational defect ($x = \pm l$) and directed away from (in the vicinity of the point $x = -l$) and to (in the vicinity of the point $x = l$) the

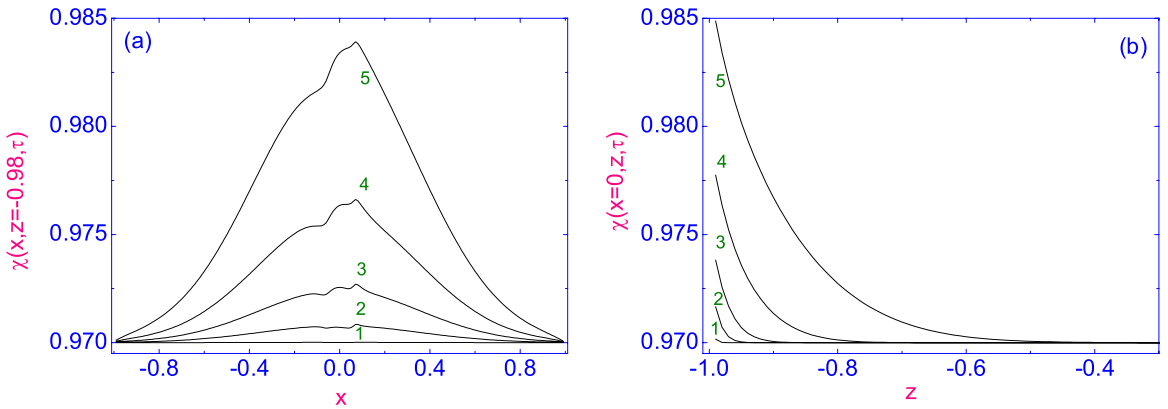

FIG. 4. (a) The relaxation of the dimensionless temperature $\chi(x, z = -0.98, \tau)$ to its stationary distribution $\chi(x, z = -0.98, \tau = \tau_{\rm in})$ along the fragment of the width $(-1.0 \leqslant x \leqslant 1.0, z = -0.98)$ of the HAN channel, at different times $\tau_1 = 10^{-7}$ ($\sim$1 ns) [curve (1)], $\tau_2 = 1.6\times10^{-6}$ ($\sim$2.8 μs) [curve (2)], $\tau_3 = 6.4\times10^{-6}$ ($\sim$11.2 μs) [curve (3)], $\tau_4 = 2.56\times10^{-5}$ ($\sim$45 μs) [curve (4)], and $\tau_5 = \tau_{\rm in} = 10^{-4}$ ($\sim$0.18 ms) [curve (5)]. (b) The same as in (a), but the relaxation of $\chi(x = 0, z, \tau)$ to its stationary distribution $\chi(x = 0.0, z, \tau = \tau_{\rm in})$ across the middle part ($x = 0$) of the HAN channel.

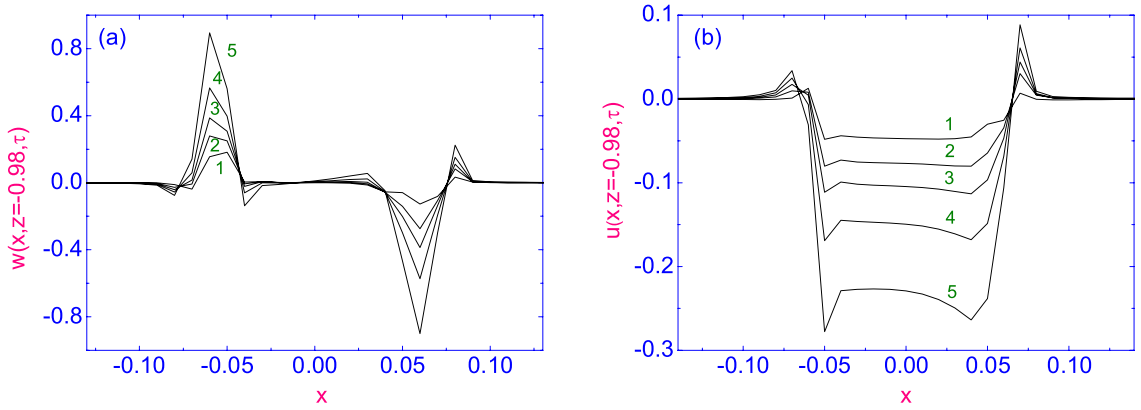

FIG. 5. (a) The relaxation of the vertical component of the velocity $w(x, z = -0.98, \tau)$ to its stationary distribution $w(x, z = -0.98, \tau = \tau_{in})$ along the fragment of the width $(-0.15 \leqslant x \leqslant 0.15, z = -0.98)$ of the HAN channel, at different times $\tau_1 = 10^{-7}$ ($\sim$1 ns) [curve (1)], $\tau_2 = 1.6\times10^{-6}$ ($\sim$2.8 μs) [curve (2)], $\tau_3 = 6.4\times10^{-6}$ ($\sim$11.2 μs) [curve (3)], $\tau_4 = 2.56\times10^{-5}$ ($\sim$45 μs) [curve (4)], and $\tau_5 = \tau_{in} = 10^{-4}$ ($\sim$0.18 ms) [curve (5)]. (b) The same as in (a), but for the horizontal component of the velocity $u(x, z = -0.98, \tau)$.

heated surface [see Fig. 5(a)], whereas in the vicinity of the middle part of the lower boundary $(-l + \delta < x < l - \delta, z = -0.98)$, the thermally excited flow is characterized by very small vertical component of the vector **v** [see Fig. 5(a)], directed in the positive sense. In turn, in that case there is the bigger horizontal flow directed in the negative sense [see Fig. 5(b)].

So, according to our calculations in case A, in which the angle θ is varied between values $\theta_{-10.0\leqslant x\leqslant -l, z=-1.0} = \theta_{l\leqslant x\leqslant 10.0, z=-1.0} = 0$, both at the left- and right-hand sides of the lower hotter boundary and $\theta_{-l<x<l, z=-1.0} = \frac{\pi}{2}$ in the middle part of the lower boundary of the HAN channel, under the influence of $\nabla\chi$, the vortical flow is settled down. Thus, the thermally excited flow is characterized by maintaining the vortex in a positive sense (clockwise) around the center $x = 0.0$ of the orientational defect $(-l \leqslant x \leqslant l)$ [see Fig. 6(a)]. Notice that in case A, the evolution of the temperature is characterized by asymmetric profile of $\chi(x, z, \tau)$ with respect to the middle part $(x = 0.0)$ of the HAN channel [see Fig. 4(a)]. It is clear that the temperature's asymmetry is caused by accounting the strong gradient $\nabla\hat{\mathbf{n}}$ along the x-direction on the lower boundary [see Eq. (3)], which is reflected in the formation of the horizontal flow of LC material near the orientational defect. In that case, during the heat step [$\tau_5 = \tau_{in} = 10^{-4}$ ($\sim$0.18 ms)], the evolution of the temperature $\chi(x, z, \tau)$ is characterized by its strong growth in the vicinity of the lower boundary up to the highest value of 0.985 ($\sim$307 K) [see Figs. 4(a) and 4(b)]. Our calculations also show that the range of distance z, counted from the lower boundary, over which the laser beam cannot perturb the nematic phase is $-0.6 \leqslant z \leqslant 1.0$, i.e., approximately 80% of the HAN channel. Note that the duration of the energy injection τ_{in} into the HAN channel is restricted only by the nematic phase stability. Further calculations (cooling regime), based on the nonlinear extension of the Ericksen-Leslie theory, show that the LC material settles down to the rest, during the time $\tau_{11} = \tau_R = 0.0064$ ($\sim$11.6 ms), after switching off the laser power, where both the horizontal $u(x, z, \tau)$ and vertical $w(x, z, \tau)$ components of the vector **v** are equal to zero, and the temperature field $\chi(x, z, \tau)$ across the LC sample is finally a downfall to the value on the upper and two lateral boundaries.

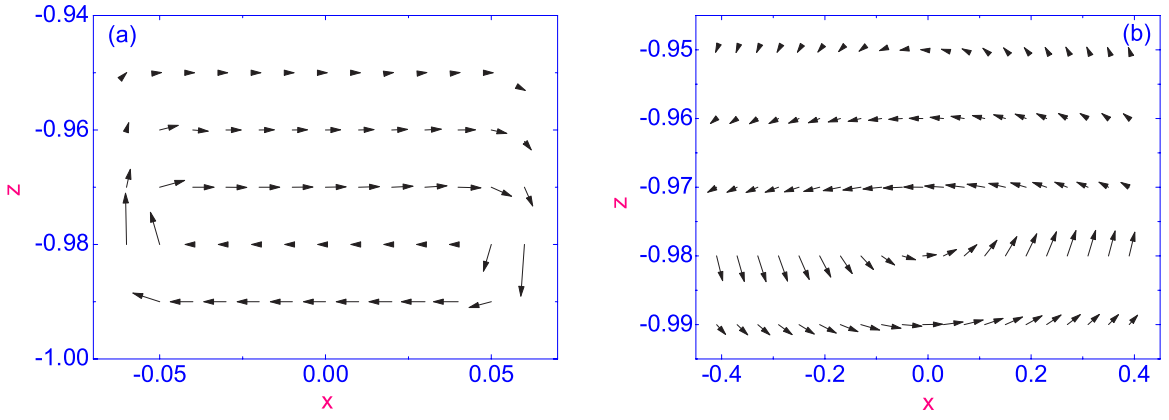

FIG. 6. (a) Distribution of the velocity field **v** in the microsized HAN channel with the orientational defect located at $-l \leqslant x \leqslant l, z = -1.0$, when the heating occurs during $\tau_{in} = 10^{-4}$ ($\sim$0.18 ms), whereas the values of the dimensionless heat flux coefficient $\mathcal{Q}_z$ is 0.18 ($\sim 1.5\times10^{-3}$ mW/μm^2), respectively. Here 1 mm of the arrow length is equal to 1.8 μm/s. (b) The same as in (a), but without the orientational defect. Here 1 mm of the arrow length is equal to 1.3 nm/s.

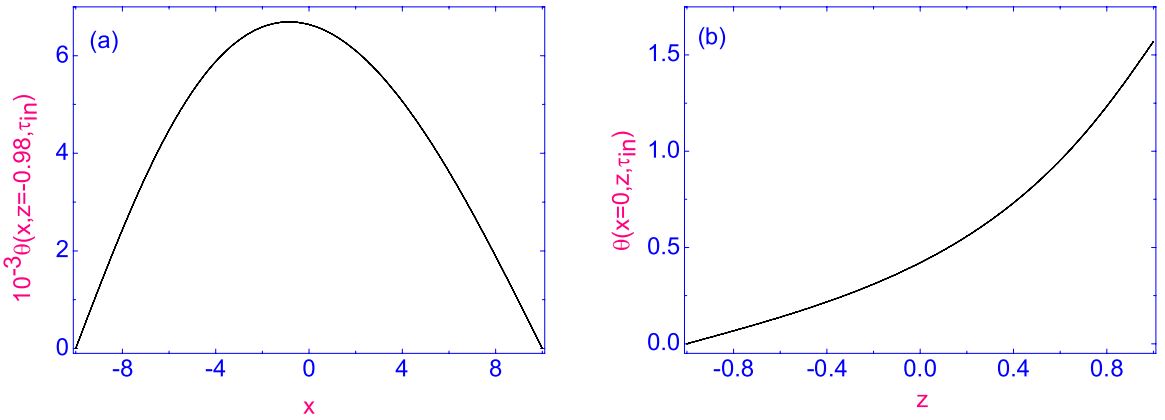

FIG. 7. (a) The stationary distribution of the polar angle $\theta(-10.0 \leqslant x \leqslant 10.0, z = -0.98, \tau = \tau_{\rm in})$ along the width $(-10.0 \leqslant x \leqslant 10.0)$ of the HAN channel, in the vicinity of the lower $(z = -0.98)$ boundary. (b) The stationary distribution of the polar angle $\theta(x = 0.0, -1.0 \leqslant z \leqslant 1.0, \tau = \tau_{\rm in})$ (in rad) across the middle part $(x = 0.0)$ of the HAN channel.

B. Case B

In order to elucidate the role of the orientational defect in maintaining of the hydrodynamic flow in the HAN channel, we have also performed the numerical study of the thermally excited fluid flow **v**, caused by the laser beam focused on a "pure" homeotropically aligned lower boundary of the HAN channel, without the orientational defect.

It can be obtained by solving the system of the nonlinear partial differential Eqs. (7), (15), and (8), together with the boundary conditions in the form of Eqs. (1), (10), (11), (13), and (14) (hereafter referred to as case B). In this case $\nabla\hat{\mathbf{n}}$ consists of the weak contribution, due to the reorientation of the director field $\hat{\mathbf{n}}$ across the HAN channel. The calculations of the polar angle $\theta(x, z, \tau = \tau_{\rm in})$ both along the width $(-10.0 \leqslant x \leqslant 10.0, z = -0.98)$ [see Fig. 7(a)] and across $(-1.0 \leqslant z \leqslant 1.0, x = 0.0)$ [see Fig. 7(b)] the HAN channel, when the heating occurs during some time $\tau_5 = \tau_{\rm in}$, are shown in Fig. 7. According to these calculations, the value of the polar angle gradually increases to the value of the right angle at the upper boundary of the HAN channel. In turn, during the heating of the microsized HAN channel without the orientational defect by laser radiation with the values of the dimensionless heat flux coefficient $\mathcal{Q}_z d/T_{NI}\lambda_\perp = 0.18$ $(\sim 1.5\times10^{-3}$ mW/μm$^2)$ and the dimensionless injection time $\tau_{\rm in} = t_{\rm in}/t_T = 10^{-4}$ $(\sim 0.18$ ms), respectively, and focused on the lower boundary at the point $x = 0.0$, the evolution of the director field $\chi(x, z, \tau)$ is characterized by its strong growth in the vicinity of the lower boundary up to the highest value of 0.988 $(\sim 307$ K) [see Figs. 8(a) and 8(b)]. Our calculations also show that the range of distance z, counted from the lower boundary, over which the laser beam cannot perturb the nematic phase, is $-0.5 \leqslant z \leqslant 1.0$, i.e., approximately 75% of the HAN channel [see Fig. 8(b)]. Note that the duration of the energy injection $\tau_{\rm in}$ into the HAN channel is restricted only by the nematic phase stability. The relaxation of both the vertical $w(x, z, \tau)$ and the horizontal $u(x, z, \tau)$ components of the velocity $\mathbf{v} = u(x, z, \tau)\hat{\mathbf{i}} + w(x, z, \tau)\hat{\mathbf{k}}$ to their stationary distributions $w(x, z, \tau = \tau_{\rm in})$ and $u(x, z, \tau = \tau_{\rm in})$, respectively, are shown in Figs. 9(a) and 9(b). In that case, on the one hand, the relaxation process is characterized by symmetric profile of the horizontal component $u(x, z, \tau)$ of the vector **v** [see Fig. 9(a)], and, on the other hand, by asymmetric profile of the vertical component $w(x, z, \tau)$ of the vector **v** with respect to the middle part $(x = 0.0)$ of the HAN channel [see Fig. 9(b)].

Symmetric evolution of the temperature field $\chi(x, z, \tau)$ relative to the laser spot at the lower boundary $([-l \leqslant x \leqslant l])$ of the HAN channel is responsible for symmetric evolution of the horizontal component of the vector **v**, whereas the evolution of the vertical component $w(x, z, \tau)$ of the vector **v** is characterized by asymmetric profile with respect to the middle part $(x = 0.0)$ of the HAN channel. Such evolution of the thermally excited flow $\mathbf{v} = u(x, z, \tau)\hat{\mathbf{i}} + w(x, z, \tau)\hat{\mathbf{k}}$ is characterized by maintaining of the smaller than in the case A vortical flow in the negative sense (anticlockwise) around their center $x = 0.0$, and in the vicinity of the lower hotter boundary $(-0.4 \leqslant x \leqslant 0.4)$ [see Fig. 6(b)]. In case B the evolution of vector $\mathbf{v} = u(x, z, \tau)\hat{\mathbf{i}} + w(x, z, \tau)\hat{\mathbf{k}}$ is characterized by very small values of these two components. Indeed, the maximum of the absolute magnitudes of both dimensionless velocities u and w, at the final stage of the heating process, occurs during the same time $\tau_5 = \tau_{\rm in}$, and are equal to 1.4×10^{-3} $(\sim 40$ nm/s) and 3.7×10^{-5} $(\sim 1$ nm/s), in case B, and 0.28 $(\sim 7.8\ \mu$m/s) and 0.91 $(\sim 25.5\ \mu$m/s), in case A, respectively.

It is clear that in case A, the localization of the vortex flow is mainly related to taking into account the strong gradient of the director field near the orientation defect. So the difference between the vortical flows in cases A and B lies not only in the directions of these thermally driven flows, but also in the magnitudes of the speeds of these flows.

Thus, the conformational *trans-cis* and *cis-trans* transitions at the lower boundary of the HAN channel crucially changes the character of the vortex flow formed under the action of focused laser radiation.

IV. CONCLUSION

The reorientation dynamics in a microsized hybrid aligned nematic (HAN) channel under the action of laser radiation focused on the lower boundary of the channel is investigated. We investigated two cases, the first, when laser radiation initiates

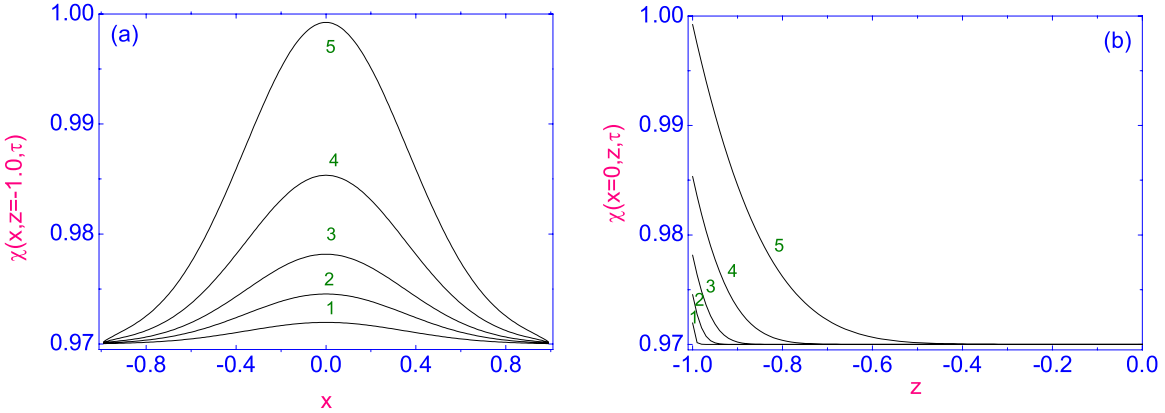

FIG. 8. (a) The relaxation of the dimensionless temperature $\chi(x, z = -0.98, \tau)$ to its stationary distribution $\chi(x, z = -0.98, \tau = \tau_{in})$ along the fragment of the width $(-1.0 \leqslant x \leqslant 1.0, z = -0.98)$ of the HAN channel, at different times $\tau_1 = 10^{-7}$ ($\sim$1 ns) [curve (1)], $\tau_2 = 1.6\times10^{-6}$ ($\sim$2.8 μs) [curve (2)], $\tau_3 = 6.4\times10^{-6}$ ($\sim$11.2 μs) [curve (3)], $\tau_4 = 2.56\times10^{-5}$ ($\sim$45 μs) [curve (4)], and $\tau_5 = \tau_{in} = 10^{-4}$ ($\sim$0.18 ms) [curve (5)], respectively. (b) The same as in (a), but the relaxation of $\chi(x = 0.0, z, \tau)$ to its stationary distribution $\chi(x = 0.0, z, \tau = \tau_{in})$ across the middle part ($x = 0.0$) of the HAN channel.

a conformational *trans-cis* transition in a Gaussian spot (case A), while in the second case (case B) this transition is absent. In turn, this conformational transition is responsible for the formation of an orientational defect at the lower boundary of the HAN channel. A mechanism is proposed to simultaneously set up the temperature gradient $\nabla\chi$ and complicate the gradient of the director $\nabla\hat{\mathbf{n}}$, consisting of the existing contribution due to the hybrid alignment of the nematic phase and the additional contribution due to the variation of the director field $\hat{\mathbf{n}}$ along the local region containing the orientational defect. This is the photoalignment mechanism that uses light-induced *trans-cis* and *cis-trans* conformational changes on the surface of azobenzene layers deposited at the boundaries of the microsized LC channel. It is shown that the charge separation during the conformational changing caused by laser irradiation may lead to the change of the surface alignment of 5CB molecules, from homeotropic to plannar and vice versa [9]. In our case there is the initially homeotropic alignment of the director along the lower boundary of the HAN channel, corresponding to the *trans*-conformational state. After laser radiation focused on the lower boundary, a small domain with a planar alignment of the director corresponding to the *cis*-conformational state should appear in the frame of the Gaussian laser spot. In this case, there is a sharper reorientation of the director field along the lower boundary of the HAN channel, especially near the boundaries of the laser spot, than across the HAN channel.

Our calculations, based on the appropriate nonlinear extension of the classical Ericksen-Leslie theory, supplemented by thermomechanical correction of the shear stress and Rayleigh dissipation function, as well as with accounting the entropy balance equation, show that due to interaction between ∇T and the gradient of the director field $\nabla\hat{\mathbf{n}}$ in the HAN channel with the orientational defect on the lower hotter boundary, a thermally excited vortical fluid flow is maintained in the vicinity of the orientational defect, with the motion in the positive sense (clockwise) around the middle part of that defect. In the case of the same HAN channel and the same heating

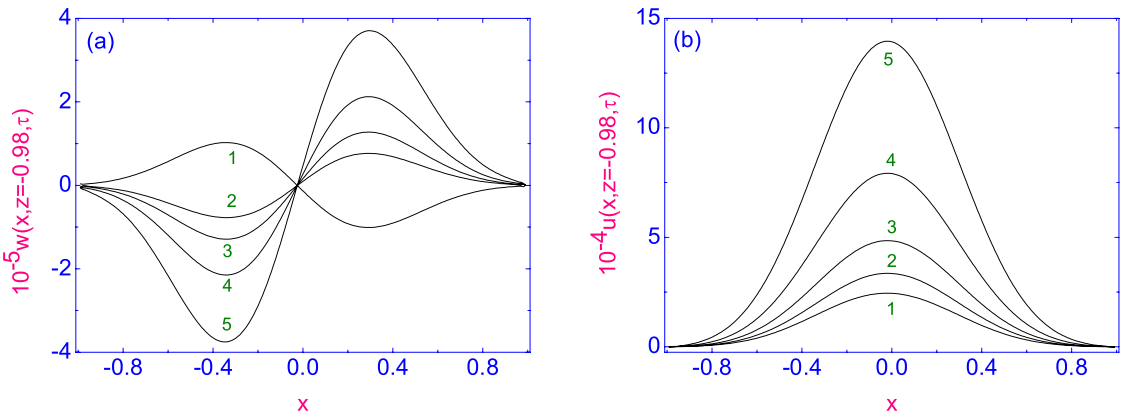

FIG. 9. (a) Plot of the relaxation of the vertical component of the velocity $w(x, z = -0.98, \tau)$, in case B, to its stationary distribution $w(x, z = -0.98, \tau = \tau_{in})$ along the fragment of the width $(-1.0 \leqslant x \leqslant 1.0, z = -0.98)$ of the HAN channel, at different times $\tau_1 = 10^{-7}$ ($\sim$1 ns) [curve (1)], $\tau_2 = 1.6\times10^{-6}$ ($\sim$2.8 μs) [curve (2)], $\tau_3 = 6.4\times10^{-6}$ ($\sim$11.2 μs) [curve (3)], $\tau_4 = 2.56\times10^{-5}$ ($\sim$45 μs) [curve (4)], and $\tau_5 = \tau_{in} = 10^{-4}$ ($\sim$0.18 ms) [curve (5)], respectively. (b) The same as in (a), but for the horizontal component of the velocity $u(x, z = -0.98, \tau)$.

regime, but without the orientational defect on the lower hotter boundary, that heating can also produce the vortical flow in the vicinity of the lower boundary, but with the motion in the negative sense (anticlockwise) around the middle part of that boundary. At that, the second vortex is characterized by a much slower speed than the vortical flow in the first case.

So, based on our calculations, one can conclude that the orientational defect on the heated boundary plays a crucial role in maintaining the thermally excited vortical flow in 2D nematic channels.

ACKNOWLEDGMENT

The reported study was funded by RFBR (RU) and DFG (GE), 20-52-12040.

[1] G. M. Whitesides, Nature (London) **442**, 368 (2006).
[2] S. J. Woltman, G. D. Jay, and G. P. Crawford, Nat. Mater. **6**, 929 (2007).
[3] A. D. Rey, Soft Matter **6**, 3402 (2010).
[4] R. B. Schoch, J. Han, and P. Renaud, Rev. Mod. Phys. **80**, 839 (2008).
[5] T. M. Squires and S. R. Quake, Rev. Mod. Phys. **77**, 977 (2005).
[6] A. P. H. J. Schenning, G. P. Crawford, and D. J. Broer, *Liquid Crystal Sensors* (CRC Press, Boca Raton, FL, 2018).
[7] A. V. Zakharov and A. A. Vakulenko, J. Chem. Phys. **127**, 084907 (2007).
[8] M. C. Gross and P. C. Hohenberg, Rev. Mod. Phys. **65**, 851 (1993).
[9] A. V. Zakharov, D. Taguchi, T. Manaka, and M. Iwamoto, J. Chem. Phys. **124**, 024701 (2006).
[10] A. Eremin, H. Nadasi, P. Hirankittiwong, J. Kiang-Ia, N. Chattham, O. Haba, K. Yonetake, and H. Takezoe, Liq. Cryst. **45**, 2121 (2018).
[11] R. S. Akopyan and B. Y. Zeldovich, Sov. Phys. JETP **60**, 953 (1984).
[12] A. V. Zakharov and A. A. Vakulenko, Phys. Rev. E **80**, 031711 (2009).
[13] E. Varneuil, M. L. Cordero, F. Gallaire, and Ch. Baroud, Langmuir **25**, 5127 (2009).
[14] A. V. Zakharov, A. A. Vakulenko, and M. Iwamoto, J. Chem. Phys. **132**, 224906 (2010).
[15] A. V. Zakharov and A. A. Vakulenko, Phys. Fluids **24**, 073102 (2012).
[16] H. Choi and H. Takezoe, Soft Matter **12**, 481 (2016).
[17] A. V. Zakharov and P. V. Maslennikov, Phys. Rev. E **96**, 052705 (2017).
[18] A. V. Zakharov and A. A. Vakulenko, Phys. Fluids **27**, 062001 (2015).
[19] A. V. Zakharov and P. V. Maslennikov, Phys. Rev. E **99**, 032701 (2019).
[20] H. Mao, J. R. Arias-Gonszalez, S. B. Smith, I. Tinoco, and C. Bustamante, Biophys. J. **89**, 1308 (2005).
[21] J. L. Ericksen, Arch. Ration. Mech. Anal. **4**, 231 (1960).
[22] F. M. Leslie, Arch. Ration. Mech. Anal. **28**, 265 (1968).
[23] L. D. Landau and E. M. Lifshitz, *Fluid Mechanics* (Pergamon Press, Oxford, 1987).
[24] N. V. Madhusudana and R. B. Ratibha, Mol. Cryst. Liq. Cryst. **89**, 249 (1982).
[25] A. G. Chmielewski, Mol. Cryst. Liq. Cryst. **132**, 339 (1986).
[26] M. Marinelli, A. K. Ghosh, and F. Mercuri, Phys. Rev. E **63**, 061713 (2001).
[27] P. Jamee, G. Pitsi, and J. Thoen, Phys. Rev. E **66**, 021707 (2002).
[28] A. A. Samarskij and E. S. Nikolaev, in *Numerical Method for Grid Equations* (Birkhäuser, Basel, 1988), p. 284.
[29] I. S. Berezin and N. P. Zhidkov, *Computing Methods*, 4th ed. (Pergamon Press, Oxford, 1965).